Chemical Gating with Nanostructured Responsive Polymer Brushes: Mixed Brush *versus* Homopolymer Brush

Mikhail Motornov, Roman Sheparovych, Evgeny Katz,* and Sergiy Minko*

Department of Chemistry and Biomolecular Science, Clarkson University, 8 Clarkson Avenue, Potsdam, New York 13699-5810

ABSTRACT In this report, we describe a novel approach to create an electrochemical gating system using mixed polymer brushes grafted to an electrode surface, and we explore the switchable properties of these mixed polymer brushes. The morphological transitions in the mixed polymer brushes associated with the electrode surface result in the opening, closing, or precise tuning of their permeability for ion transport through the channels formed in the nanostructured thin film in response to an external stimulus (pH change). The gating mechanism was studied by atomic force microscopy, ellipsometry, contact angle measurements, force–distance measurements, and electrochemical impedance spectroscopy. In comparison to a homopolymer brush system, the mixed brush demonstrates much broader variation of ion transport through the thin film. We suggest that this approach could find important applications in electrochemical sensors and devices with tunable/switchable access to the electrode surface.

KEYWORDS: polymer brush · responsive materials · electrochemical gate · ion channel · thin film

Chemical gates are very important components of biological systems associated with biomembranes and are used for transporting ions or molecules across cell membranes.[1–6] The chemical gates are usually composed of special proteins embedded in the biomembranes that provide channels for the controlled transport of ions or molecules. The ion/molecular transport regulation (opening and closing of channels) is triggered by interactions between the channel proteins and signaling molecules or ions, or in response to other physical signals, such as changes in the electrical potential on the membrane. The transmembrane chemical gates (molecular/ion channels) perform important physiological functions involved in sensing, signal transduction, and energy conversion. Artificial systems have been designed that mimic these biochemical gates. Some of these artificial systems use natural membrane proteins implanted into artificial membranes[7,8] or matrices,[9–11] while others use fully artificial synthetic polymeric materials to simulate the function of natural biochemical gates.[12–17]

In this paper we mimic natural gating devices, exploring responsive polymer brushes. Polymer brushes are responsive thin films capable of switching their morphology in response to various external stimuli *via* different phase-segregation mechanisms. Here, the term "brush" denotes a layer of polymer chains tethered to a solid substrate (Figure 1a,b); the high grafting density obliges the polymers to stretch away from the grafting surface.[18,19] In the case of binary (mixed) brushes (Figure 1c–f), two disparate polymers are grafted onto the substrate in a random pattern.[20,21] These two polymers are segregated and form nanosize phases that scale with the mean chain end-to-end distances.[22] Changes in the surrounding environment, such as the thermodynamic quality of solvent,[23–26] humidity,[27] pH,[28] or temperature,[29,30] can promote switching between various phase-segregated morphologies. These changes can also affect the chemical composition of the top layer of the polymer brush. The unique behavior of polymer brushes has attracted much recent interest for use in various applications, such as microfluidic devices,[31,32] responsive colloids,[33,34] "smart" coatings,[35,36] responsive fabrics,[37] protein adsorption materials,[38] and supports for directed assembly of nanoparticles.[39]

Huck *et al.*[40,41] have recently investigated homopolymer brushes (comprising a single type of polymer chain) using Faradaic impedance spectroscopy. They demonstrated that homopolymer polyelectrolyte brushes have switchable electron-transfer resistance. The swollen quaternized

*Address correspondence to ekatz@clarkson.edu, sminko@clarkson.edu.

Received for review September 7, 2007 and accepted November 29, 2007.

Published online December 19, 2007.
10.1021/nn700214f CCC: $40.75

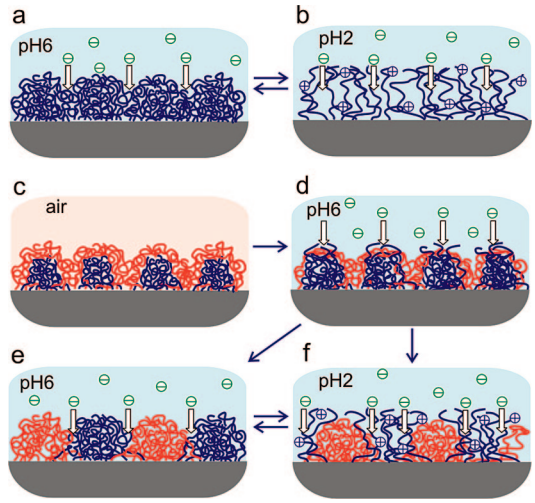

Figure 1. pH-responsive homopolymer polycationic (P2VP) brush (a,b) *versus* the mixed brush (c−f) prepared from PDMS and P2VP, both in a collapsed (noncharged) state in air or in a poor solvent (a,c,e) and in an ionized swollen state (b,d,f). The homopolymer brush forms pinned micelles in the collapsed state (a) and is swollen and permeable for anions (green arrows) in the protonated state at pH 2 (b). The mixed brush is sealed by the topmost PDMS (polymer A) layer in air (c) and partially coated by PDMS in water at pH 6 (d). The mixed brush is permeable for anions due to swollen P2VP (polymer B) chains at pH 2 (f) and returns in the state with a poor permeability at pH 6 (e). The hysteretic behavior is seen when comparing (d) and (e).

poly[(dimethylamino)ethylmethacrylate] brush was shown to have good ion permeability, while high resistance was observed for the collapsed brush in saline solutions.

Here we study a novel property of *mixed polymer brushes* to regulate transport of ions and gate electrochemical processes. In this paper we compare the gating mechanisms for homopolymer poly(dimethylsiloxane) (PDMS, also referred to here as polymer A) and poly(2-vinylpyridine) (P2VP, also referred to here as polymer B) brushes with the gating properties of the mixed PDMS/P2VP brush. We demonstrate that the mixed brush offers remarkable and versatile opportunities for chemical gating. The results of this study indicate that the mechanisms of phase transition differ in homopolymer and mixed brushes. In both cases, the mechanism depends on the reduced grafting density, Σ (the number of chains that occupy an area that a free, non-overlapping polymer chain would normally fill at the same experimental conditions). Here, $\Sigma = \sigma\pi(\langle s^2\rangle^{1/2})^2$, where σ is the grafting density, or the number of chains per surface unit, and $\langle s^2\rangle^{1/2}$ is the root-mean-square (rms) radius of gyration of the tethered chain at specific experimental conditions of solvent and temperature. Homopolymer brushes were shown to have a homogeneous swollen morphology in good solvents (Figure 1b). A change of the solvent quality from a "good" solvent to a "poor" solvent resulted in shrinkage of the initially swollen layer. At low and moderate grafting densities ($1 \leq \Sigma < 10$), homopolymer brushes formed the laterally segregated structures (pinned micelles) shown in Figure 1a in order to avoid unfavorable interactions with the poor solvent.[42] The size of the micelle is balanced by the interaction energy from one side and the elastic energy of the stretched chains from the other side.

Mixed polymer brushes from incompatible polymers A and B adopted a laterally segregated morphology in all solvents tested (Figure 1c−f).[22,43–48] In a common (nonselective) good solvent, a symmetric (by composition [A]:[B] = 1 and molecular mass) mixed brush forms a ripple phase consisting of alternating cylindrical domains of each polymer aligned parallel to the grafting surface. The transition from the ripple phase to asymmetric dimple-A and dimple-B phases occurred following changes in solvent selectivity, further increases of incompatibility between the two polymers, or a change of the brush composition to asymmetric. The dimple phases consist of round clusters of one polymer arranged in a hexagonal lattice and surrounded by the matrix of the second polymer. In selective solvents, the insoluble polymer forms clusters segregated to the grafting surface, while the soluble polymer dominates in the surrounding matrix (Figure 1f). Thus, the concentration of polymer A in a poor solvent is higher near the grafting surface and lower at the brush surface. In this case, the brush layer morphology can be described as a combination of lateral and layered segregation of two polymers (A and B). This has previously been proven experimentally. [22,23,25,49–52]

Polyelectrolyte brushes represent a specific kind of polymer brush where electrostatic interactions modify the phase transition mechanism.[53] Changes in charge density of the grafted chains result in a change of the osmotic effect on the brush swelling, where swelling/shrinking polymer chains can be tuned by changing the ionic strength or pH (for weak polyelectrolytes) of the solutions. If one of the two polymers in the mixed brush is a weak polyelectrolyte, then a pH change will selectively affect the swelling/shrinking of the polyelectrolyte chains (Figure 1e,f).

A specific case of the mixed brush state can be distinguished if a solvent evaporates and the brush is dry. Typically, most dry polymers are in a glassy state at ambient conditions and the brush is "frozen" in a nonequilibrium state. A very interesting behavior was observed for liquid mixed polymer brushes in air.[27] If the polymers are in a liquid state, the phase transition takes place in a dry state and a more hydrophobic polymer occupies the brush surface (Figure 1c) contacting "hydrophobic" air. In this paper we show how the interplay between liquid−glass transitions from one side and between lateral and layered segregated phases in mixed brushes from the other side allows for a versatile regulation of the mixed brush permeability and chemical gating.

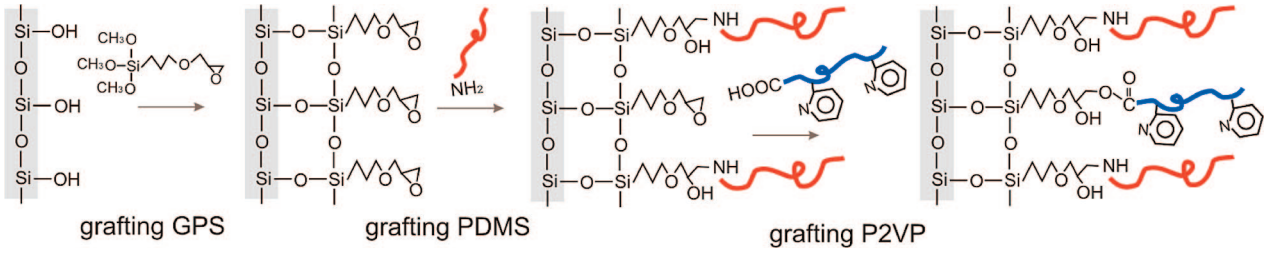

Figure 2. Grafting of the mixed brush onto the Si wafer: step 1, grafting GPS; step 2, grafting PDMS; and step 3, grafting P2VP. Here we demonstrate grafting on the Si wafer; the same scheme was applied for the ITO glass using OH functional groups on the surface.

RESULTS AND DISCUSSION

Grafting of the Mixed Polymer Brush. In the first step, 3-glycidoxypropyl trimethoxysilane (GPS) was grafted to the surface of either an indium−tin oxide (ITO) glass or Si wafers (Figure 2) according to a protocol explained in detail elsewhere.[50] The ellipsometric thickness of the GPS films of about 1.0 ± 0.1 nm corresponds to the 1 ± 0.1 theoretical monolayer of the GPS. The average surface concentration of GPS, calculated from ellipsometry data, is in the range of 3 molecules · nm^{-2}.

The next step comprises the grafting of aminopropyl-terminated poly(dimethylsiloxane) (PDMS-NH_2) from a bath with liquid polymer (Figure 2). A sample of GPS-modified substrate was dipped into the bath. The kinetics of the grafting of PDMS-NH_2 and the grafted layer morphology were recently reported in the literature.[27] The grafting time was adjusted to graft about 50% (3 nm) of the mixed brush plateau value to reserve a space for the grafting of the second polymer. The thickness found with ellipsometry was verified by an atomic force microscopy (AFM) scratch test. In this experiment, the polymer layer is scratched with an ultrasharp needle to delaminate the layer down to the Si wafer (ITO glass). The sample is then scanned over an area with the scratched line to verify the quality of the scratch and the actual thickness. The thicknesses obtained from the scratch tests are in good agreement with the ellipsometric thicknesses in both ITO and Si substrates (Table 1).

The second polymer, carboxy-terminated poly(2-vinylpyridine) (P2VP-COOH), was grafted from the melt (Figure 2) as described elsewhere.[50] A thin (*ca.* 50–100 nm) P2VP-COOH film was spin-cast on the substrates with grafted PDMS brushes and annealed at 130 °C. The grafting from the melt was also used to prepare reference samples of the P2VP homopolymer brush. The grafting was followed by multiple washings with water, acidic water at pH 3, and methyl ethyl ketone (MEK).

The molecular characteristics of the brushes, as evaluated by ellipsometric and AFM scratch tests, are given in Table 1. The total grafting density, σ, for all the brushes is close to 0.1 chain · nm^{-2}. The distance between grafting points, L_g (calculated as $L_g = 2(\pi\sigma)^{-1/2}$), is smaller than the corresponding thickness of the brush, H. Consequently, even in the dry samples, the grafted chains are stretched away from the grafting surface and the layer is in the brush regime. Reduced grafting density, Σ, was evaluated for the θ conditions, and the values were $\Sigma \gg 1$ for all samples. Thus, the brushes are considerably stretched in θ and good solvents.

Switchable Morphology of the Polymer Brushes. Ellipsometric mapping shows the macroscopic homogeneity of the brushes. The microscopic morphology of the PDMS homopolymer brush grafted to the Si wafer was visualized with AFM (Figure 3a,b). The film appears as a macroscopically homogeneous flat thin film with segregated domains (clusters with a 53 ± 6 nm diameter, rms roughness of 1.4 nm)[27] that indicate the dimple (pinned micelles) regime of the brush.[54] The morphology was not changed upon immersion of the sample in water at pH ranging from 2 to 6.

The morphology of the P2VP homopolymer brush in water at pH 6 is shown in Figure 3c,d. Similar to the

TABLE 1. Molecular Characteristics of the Samples of Mixed Brushes and Reference Homopolymer Brushes Prepared on ITO Glass and Si Wafer Substrates

polymer brush sample	thickness of brush, H, nm: ellipsometry ±0.2 nm	thickness of brush, H, nm: AFM scratch ±0.5 nm	grafted amount, A ±0.2 mg · m^{-2}	composition P2VP:PDMS, ±5% mass	σ, ±0.01 nm^{-2}	L_g, ±0.2 nm	Σ, ±1
mixed on ITO	6.2	7.1	6.7	59:41	0.10	3.6	7.4
mixed on Si	5.7	5.1	5.3	47:53	0.09	3.7	7.0
PDMS on ITO	5.8	5.3	5.7	100[a]	0.11	3.3	5.2
PDMS on Si	4.0	3.9	3.9	100[a]	0.08	4.0	3.6
P2VP on ITO	6.2	5.9	7.3	100[b]	0.08	4.0	8.8
P2VP on Si	7.0	6.7	8.9	100[b]	0.09	3.8	9.9

[a]PDMS. [b]P2VP.

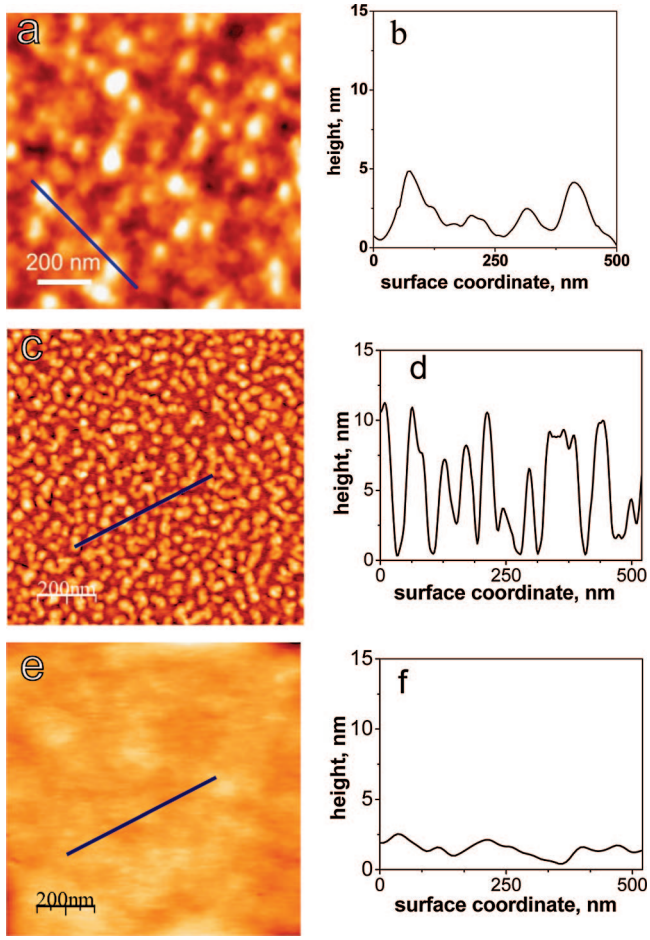

Figure 3. AFM topographical images (a,c,e) and cross-sections (b,d,f) of the reference homopolymer brushes from PDMS (brush thickness 3.9 nm) in air, rms roughness 1.4 nm (a,b); P2VP (brush thickness 6.7 nm) in water at pH 6, rms roughness 3.3 nm (c,d); and P2VP (brush thickness 6.7 nm) in water at pH 2, rms roughness 1.1 nm (e,f).

PDMS brush, the P2VP brush in the poor solvent adopts the pinned micelle morphology. The brush was only slightly swollen in water, and the morphology was the same as that of the dried sample. Lowering the pH from 6 to 2 caused a dramatic change in the P2VP brush morphology due to osmotic swelling of the ionized pyridine groups and counterions. The brush swelled from 6.5 to 17 nm (ellipsometric thickness), and AFM revealed that it was a smooth layer with rms roughness of 1.1 nm (Figure 3e,f). This transition is in good agreement with the model depicted in Figure 1a,b. The transition is reversible and was repeated many times.

The AFM images (Figure 4) reveal lateral nanoscale phase segregation in the *mixed brush* in a dry state and in aqueous environments at different pH values. Water is a much poorer solvent for PDMS than for P2VP. Hence, PDMS forms clusters embedded in the P2VP matrix at all pH values tested. The P2VP matrix shrinks (6 nm ellipsometric thickness) at pH 6 and swells (12 nm ellipsometric thickness) at pH 2 (compare cross-section images b and d in Figure 4). We investigated the structure in detail to find out whether these changes affect laterally segregated PDMS domains in such a way that the fraction of the solid surface coated by PDMS is changed. The latter could take place if swollen P2VP chains deform and push the PDMS clusters away from the grafting surface. Subtraction of image a from image c, as shown in Figure 4e, results in a smooth surface with a low roughness (Figure 4f). Using the "flooding mode" of the commercial software, we have estimated the volume of the segregated PDMS clusters at pH 6 and at pH 2 to be $(5.5 \pm 1) \times 10^5$ nm^3 in both cases. The volume of the clusters in the subtracted image (Figure 4e) is 20-fold smaller (*ca.* 2×10^5 nm^3). Thus, changes in the shape of PDMS clusters are negligibly small (since a noticeable change in the cluster shape would result in a higher "residual" volume of structures in the subtracted image). The mixed brush behavior is consistent with the model shown in Figure 1e,f.

We may conclude that changes in pH causes the *homopolymer brush* to reversibly switch morphology in aqueous solutions, from a stretched homogeneous brush-like layer to a collapsed monolayer of pinned micelles. This is in contrast to the behavior of the *mixed brush*. In the mixed brush, the laterally segregated PDMS domains remain unchanged, while the P2VP brush domains reversibly swell and shrink in the *Z*-direction in response to changes in pH (compare cartoons a,b and e,f in Figure 1).

Wettability Switching Probed by Contact Angle. Contact angle measurements are very sensitive to the very top composition of a thin film. This method was successfully used to investigate switching mechanisms in mixed polymer brushes.[20] If polymers are in a glassy state in air at room temperature, then the contact angle is very sensitive to the sample history. If the mixed brush was pre-exposed to a solvent, then rapid evaporation of solvent results in a collapse of the polymer film in the *Z*-direction. The segregated domains of the glassy polymer in the dry sample store the information about the morphology of the brush in the solvent used for the pretreatment of the sample. Thus, pretreatment of the mixed brush with different solvents resulted in changes of the morphology stored in the dry sample and, hence, in the tunable wetting behavior of the brush samples.[23] This morphology can be probed with contact angle experiments.

If the polymers of the mixed brush are in the liquid state, the brush adopts equilibrium morphology in air. This morphology typically is a combination of laterally segregated domains with the morphology of stratified polymers. Two incompatible polymers segregate laterally, and the most hydrophobic polymer tends to occupy the top layer.[27]

In our present case of the PDMS/P2VP brush, PDMS is in the liquid state and tends to occupy the top layer in air. The data of the contact angle experiments are summarized in Table 2. We show here the data obtained for the samples on Si wafers. We observed the same results for the samples prepared on the ITO glass.

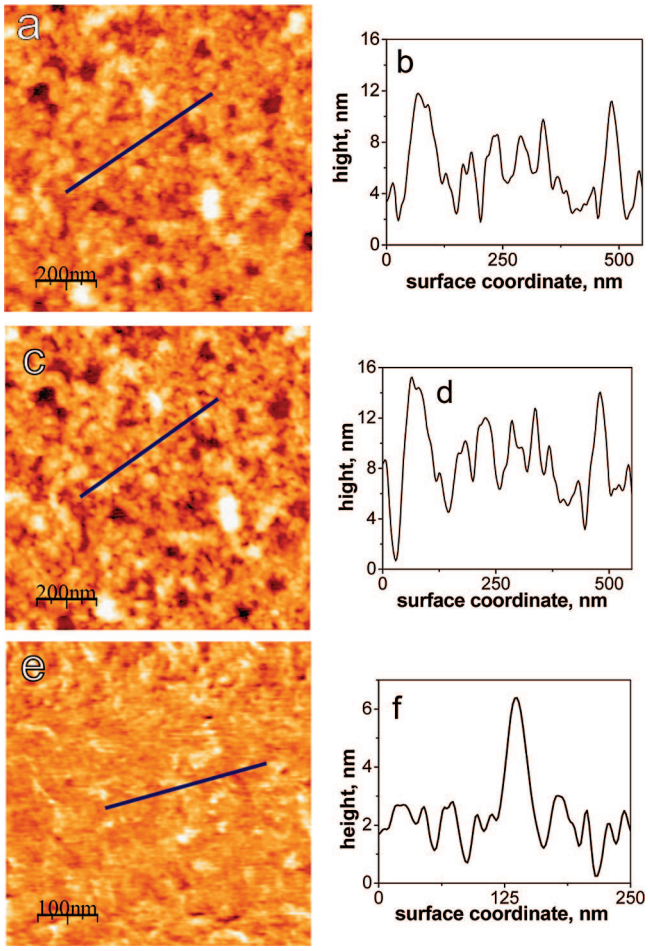

Figure 4. AFM topographical images (a,c,e) and their cross-sections (b,d,f) of the PDMS/P2VP mixed brush on the Si wafer in aqueous solution at pH 6, $H = 6$ nm, rms roughness 4.1 nm (a,b), and at pH 2, $H = 12$ nm, rms roughness 3.9 nm (c,d). Image e was obtained by subtraction of image a from image c, rms roughness 1.0 nm (f).

The reference homopolymer PDMS brush demonstrates hydrophobic behavior (103–106° advancing angles) with a very small wetting hysteresis (91–97° receding angles) for all pretreatment conditions. The homopolymer P2VP brush shows (i) very high wetting hysteresis (68–77° advancing angles) *versus* 33–38° receding angles due to the reconstruction of the top layer in water (change of the space distribution of pyridine rings, which tend to contact the water phase) and (ii) a very pronounced change of wetting behavior upon pretreatment with acidic solution (77° after treatment with water at pH 6 *versus* 26° after treatment with water at pH 2) due to protonation of pyridine rings. Thus, there is a drastic difference between the properties of the PDMS and P2VP homopolymer brushes that can be used to probe the surface morphology of the mixed brush.

The mixed PDMS/P2VP brush is more hydrophobic than the P2VP brush (95–97° for the mixed brush *versus* 68–77° for the P2VP brush) and demonstrates much larger wetting hysteresis than the PDMS brush (Figure 5).

In contrast to the earlier reports of mixed brushes prepared from glassy polymers,[23] this brush shows no memory of pretreatment solvents, with one exception: pretreatment with acidic water returns a slightly more hydrophilic brush (86° after treatment with water at pH 2 *versus* 97° after treatment with water at pH 6). Thus, we may conclude that the surface of the mixed PDMS/P2VP brush is always "sealed" by a thin layer of PDMS (Figure 1c). Upon exposure to water at pH 6, the morphology changes (Figure 1d), and more P2VP chains are in contact with water. Upon further decreases in pH, the morphology switches dramatically (Figure 1f). Altering the pH in an aqueous environment results in morphological changes between the states shown in Figure 1e,f. The states shown in Figure 1c,d are specific states that can be approached for the dry sample and for the sample exposed to water at pH 6 after the dry state. We proved this conclusion by probing the surface of the mixed brush in air and in aqueous solutions with the AFM tip.

Switching Probed by Force–Distance Measurements. We probed the surface composition of the mixed brush *versus* homopolymer brushes with a SiN AFM tip in air

TABLE 2. Water Contact Angles on the Surface of the Mixed PDMS/P2VP Brush and the Reference PDMS and P2VP Homopolymer Brushes Pretreated with Different Solvents and Rapidly Dried in Air

		contact angle, ±2°	
brush sample	pretreatment	advancing	receding
PDMS	MEK	106	97
	water, pH 6	107	96
	water, pH 2	103	91
P2VP	MEK	68	33
	water, pH 6	77	38
	water, pH 2	26	26
PDMS/P2VP	toluene	95	51
	MEK	97	30
	water, pH 6	97	50
	water, pH 2	86	19

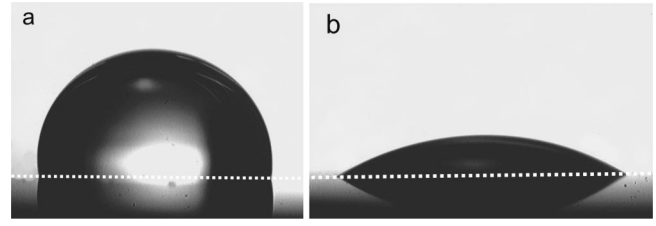

Figure 5. Advancing (a) and receding (b) contact lines for the water droplet placed on the surface of the mixed PDMS/P2VP brush. The dotted line marks the locus of the contact lines.

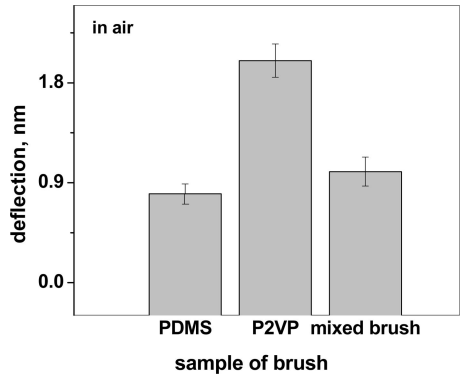

Figure 6. AFM cantilever deflection (with error bars) in air upon retraction from the surface of the mixed PDMS/P2VP brush and the reference P2VP and PDMS homopolymer brushes.

and with a silicon tip modified by chemically grafted primary amino functional groups in water. In each experimental series, we used the same tip to ensure that the results (adhesion) were presented in terms of the maximal deflection of the cantilever in the retraction mode. The data collected for the brushes in air are summarized in Figure 6. The results clearly demonstrate that the level of adhesion between the tip and the mixed brush is very close to the adhesion between the tip and the PDMS brush and is much smaller than that for the P2VP brush. Consequently, the PDMS chains are exposed to the brush surface in air (Figure 1c).

In acidic aqueous solutions, P2VP chains in the brush and the amino-functionalized tip carry similar (positive) charges, and the interaction between them is strongly influenced by repulsive electrostatic forces (Figure 7). Thus, the adhesion to the charged P2VP chains is lower as compared to that for the hydrophobic PDMS due to the effect of the capillary force. After

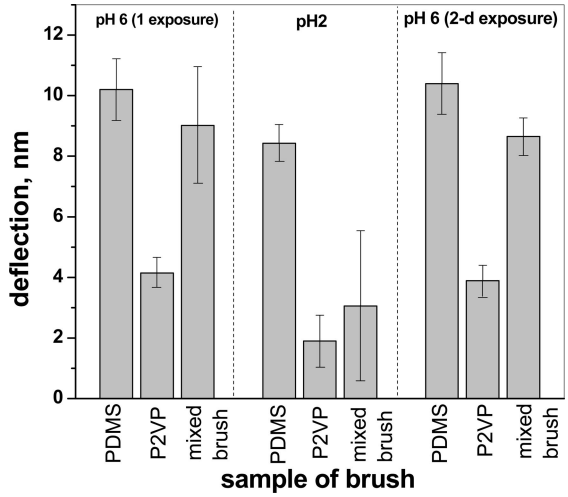

Figure 7. AFM cantilever deflection in water upon retraction from the surface of the mixed PDMS/P2VP brush and the reference P2VP and PDMS homopolymer brushes: at pH 6 after the first immersion of the dry sample in aqueous solution, at pH 2, and at pH 6 after rinsing the sample with Millipore water (the sample remained wet throughout the cycle).

the tip has contacted the sample, PDMS chains form a meniscus that exerts a strong adhesion force. Such a strong hydrophobic interaction of AFM tips with soft hydrophobic materials in water is well described in the literature.[55] We performed a cycle of treating the brush with aqueous solution at different pH values. Initially, the dry samples were immersed in water at pH 6, and then the measurements were performed in solutions at pH 2. Finally, we took another measurement of adhesion in a pH 6 solution after rinsing the sample multiple times with Millipore water. Samples remained wet throughout the entire cycle and were never allowed to dry. These three groups of measurements are shown in Figure 7.

We may conclude that the adhesion to the PDMS homopolymer brush remains unchanged at pH 6 throughout the treatment cycle. Adhesion to the PDMS homopolymer brush is lower at pH 2 than at pH 6, which can possibly be ascribed to the repulsive contribution of positively charged end amino groups used for the grafting. Adhesion to the P2VP homopolymer brush is much lower at pH 6 than that for the PDMS homopolymer brush and is very small at pH 2. This is due to the repulsive contribution of positively charged pyridine rings. This result is in good agreement with the schematic transition depicted in Figure 1a,b.

At pH 6, the mixed brush exhibits an adhesion level similar to that for the homopolymer PDMS brush at pH 6, but the adhesion level for the mixed brush at pH 2 is similar to that for the homopolymer P2VP brush at pH 2. This agrees well with the schemes shown in Figure 1e,f: at pH 2, the topmost layer is populated by swollen protonated P2VP chains, while at pH 6, sticky PDMS chains are available on the surface. In accordance with the wetting experiment, we observe a small difference between the first immersion of the mixed brush in water at pH 6 (depicted in Figure 1d) and the second immersion in water at pH 6 (depicted in Figure 1e) if the first immersion was followed by treatment with water at pH 2. This difference can be explained by the fact that water at pH 6 is a poor solvent for P2VP; therefore, the surface reconstruction for the first immersion in water at pH 6 is kinetically frozen, and the brush is in a metastable state (the brush retains in the state which corresponds to the dry sample). Swelling the brush in acidic solution results in a change of the morphology of the brush. However, increasing the pH to 6 does not return the brush to the same state that was observed for the first immersion but rather results in a new state. This new state corresponds to the equilibrium morphology of the brush at pH 6. We note here that the sequence of transitions is highly reproducible (we repeated the cyclic treatments at least 10 times) and was always observed when the brush was dried and immersed in aqueous solutions with the corresponding pH values.

Thus, we may conclude that all morphological states of the brushes depicted in Figure 1 were experimen-

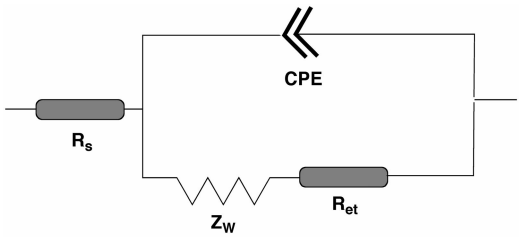

Figure 8. Equivalent circuitry used to fit the experimental Faradaic impedance spectra: R_s, ohmic resistance of the bulk electrolyte solution; R_{et}, electron-transfer resistance; CPE, constant phase element; and Z_W, diffusional Warburg impedance.

tally evidenced. On the basis of the morphological transitions in response to pH changes, we may suggest that the nanostructured film from the mixed brush could be used for chemical gating. The transport of ions from the solution to the grafting surface can be switched and tuned *via* pH changes in the aqueous solution. That was proved in the electrochemical experiments with the brushes prepared on the conductive ITO glasses.

Study of Chemical Gating with Impedance Spectroscopy. The gating properties of the polymer brushes assembled on ITO electrode surfaces were studied by Faradaic impedance spectroscopy.[56,57] This tool is used to determine blocking effects on electrode surfaces, particularly in biosensors, immunosensors, and DNA sensors.[58] The switchable/tunable operation of various electrochemical gates on polymer films was also studied by impedance spectroscopy.[59–61] The Faradaic impedance spectra were recorded in the presence of a soluble redox probe, $[Fe(CN)_6]^{3-/4-}$, thus reflecting the permeability of the polymer brush thin films in different states for the diffusional redox species. The experimentally obtained impedance spectra were presented in the form of complex plane graphs (Nyquist plots), where the semicircle domains approximately correspond to the electron-transfer resistance values, R_{et}, for the electrochemical processes. In order to derive the exact values of R_{et} from the experimental spectra, the data were fitted by a theoretical equivalent circuit characteristic of diffusion electrochemical processes proceeding at surfaces of modified electrodes (modified Randles and Ershler model,[56,57,62,63] Figure 8). This equivalent circuitry includes the ohmic resistance of the bulk electrolyte solution, R_s, electron-transfer resistance, R_{et} (actually dependent on the modifying thin film associated with the electrode surface), constant phase element, CPE (mostly reflecting the interfacial capacitance distributed in the modifying thin film), and diffusional Warburg impedance, Z_W (characterizing the diffusional charge transport through the bulk solution), as the components of the equivalent circuitry. The CPE was used instead of the double-layer capacitance, C_{dl}, reflecting the space-distributed capacitance of the thin film associated with the electrode surface.[58,64] It should be noted, however, that upon fitting the experimental data to the theoretical equivalent circuitry, the physical meaning of the CPE was shown to be very close to C_{dl}, thus justifying the use of the Randles and Ershler theoretical model. The characteristic parameter obtained from the fitting process was R_{et}, derived at different pH values and reflecting various states of the polymer brushes.

The Faradaic impedance spectra were first obtained for the electrode modified with a homopolymer (single-component) P2VP polymer brush in electrolyte solutions at different pH values. The electrolyte solution was composed of 10 mM $[Fe(CN)_6]^{3-/4-}$ and 0.1 M Na_2SO_4 at pH 6.4. The pH in the electrochemical cell was subsequently lowered by adding H_2SO_4 until the pH reached 1.8. The impedance spectra for various pH values are presented in Figure 9A in the form of Nyquist plots. The continuously decreasing diameter of the semicircle domain in the impedance spectra upon acidification of the electrolyte solution demonstrates the decrease of R_{et} for the interfacial electron transfer. This interfacial electron transfer originates from the pH-induced swelling of the polymer brush and results in the formation of ion channels. The exact values of R_{et}, derived from the impedance spectra by their fitting with the equivalent electronic circuitry (Figure 8), were plotted to yield a titration curve corresponding to the structural rearrangements in the polymer brush upon changes in the pH of the solution (Figure 9B, data set i.) The opposite titration (from pH 1.8 to pH 6.4) was performed by adding NaOH to the electrolyte solution in the electrochemical cell. The corresponding impedance spectra were recorded (not shown). These spectra were similar to the data shown in Figure 9A, and the titration curve for the shrinking process of the polymer brush upon increasing the pH value coincides with the titration curve obtained upon acidification of the solution (Figure 9B, data set ii; note the opposite directions of the R_{et} changes in the two titration curves). The titration was then repeated to again acidify the solution. The titration curve (R_{et} *versus* pH) again correlates with the previously obtained titration curves. The obtained data demonstrate the reversible character of the structural changes in the monocomponent polymer brush, which swells and shrinks as the pH decreases and increases, respectively. The open and closed states of the chemical gate made of the single-polymer P2VP brush were characterized by R_{et} values of *ca.* 610 and 320 Ω, respectively. Any value of R_{et} in this range can be obtained by the controlled variation of the pH value of the electrolyte solution.

The next step of the experiment was done using the bicomponent mixed polymer brush (PDMS/P2VP). The impedance spectra were obtained as in the previously discussed experiments, and the resulting data are represented as Nyquist plots. Figure 10A shows the impedance spectra obtained upon lowering the pH from 6.04 to 1.81. Obviously,

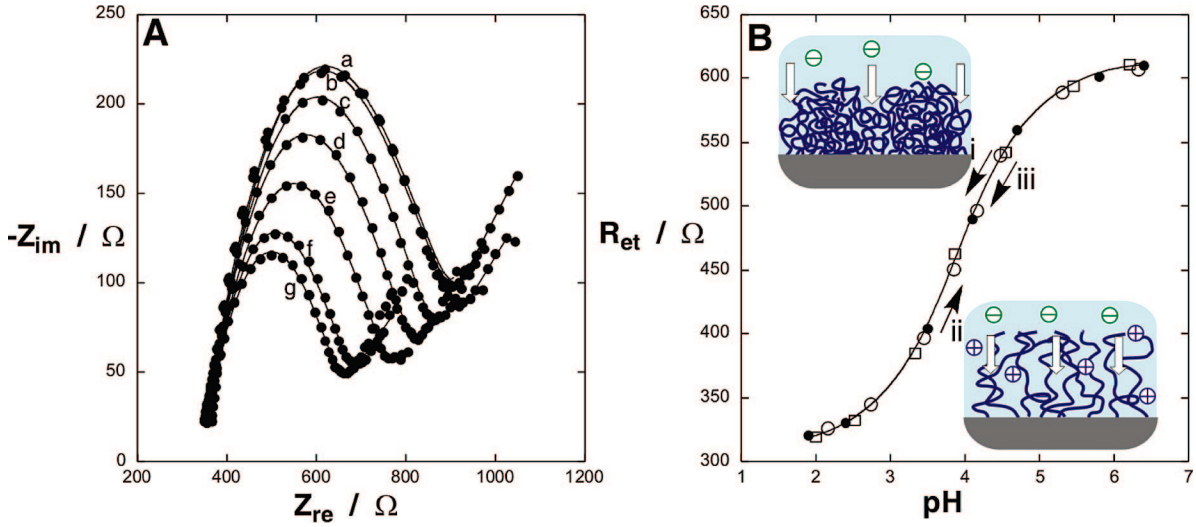

Figure 9. (A) Nyquist plot (Z_{im} *versus* Z_{re}) for the Faradaic impedance measurements performed on the P2VP brush-modified ITO electrode (solid lines correspond to the fit of the experimental points to the theoretical equivalent circuitry) obtained at different pH values: (a) 6.4, (b) 5.8, (c) 4.7, (d) 4.0, (e) 3.5, (f) 2.4, and (g) 1.8. The data were recorded in 0.1 M Na_2SO_4, in the presence of 10 mM $K_3[Fe(CN)_6]/K_4[Fe(CN)_6]$, 1:1, bias potential of 0.17 V. (B) Titration curve showing changes of the electron-transfer resistance derived from the impedance spectra upon variation of the pH value: (i) the first run of the pH value in the acidic direction (●); (ii) the second run of the pH value in the basic direction (○); and (iii) the third run of the pH value in the acidic direction (□).

acidification of the solution causes the electron-transfer resistance values to decrease (observed as the decrease of the diameter of the semicircle domain in the Nyquist plot), thus demonstrating the opening of the chemical gate on the interface. The titration curve (R_{et} *versus* pH) corresponding to the first acidification of the solution is plotted in Figure 10B, data set i, using the R_{et} values derived from the experimental impedance spectra (Figure 10A) by fitting with the theoretical equivalent electronic circuit (Figure 8). The electrolyte solution was then titrated with NaOH to raise the acidic solution to a neutral pH. The titration curve (Figure 10B, data set ii) shows hysteresis with the first titration curve from the first acidification experiment. However, the next acidification repeats the titration curve obtained upon the second titration in the basic direction (Figure 10B, data set iii). All other titration experiments result in the same highly reproducible dependence of R_{et} *versus* pH (we repeated the cycle at least 10 times); thus, the hysteresis was observed only for the difference between the very first titration in the acidic direction and the second titration in the reverse direction. It should be noted that this hysteresis is also highly reproducible when the experiment is repeated after exposing the mixed brush-modified electrode to air or a nonpolar solvent (*e.g.*, toluene) for a few minutes. This can be explained by the exposure of the nonpolar component in the mixed polymer brush to the interface upon its incubation

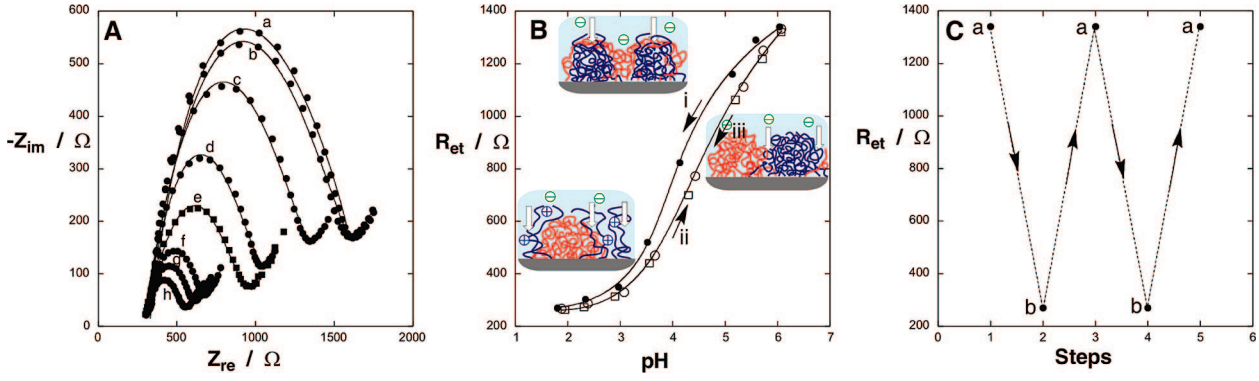

Figure 10. (A) Nyquist plot (Z_{im} *versus* Z_{re}) for the Faradaic impedance measurements performed on the PDMS/P2VP brush-modified ITO electrode (solid lines correspond to the fit of the experimental points to the theoretical equivalent circuitry) obtained at different pH values: (a) 6.04, (b) 5.60, (c) 5.07, (d) 4.08, (e) 3.50, (f) 3.01, (g) 2.25, and (h) 1.81. The data were recorded in 0.1 M Na_2SO_4 in the presence of 10 mM $K_3[Fe(CN)_6]/K_4[Fe(CN)_6]$, 1:1, bias potential of 0.17 V. (B) Titration curves showing changes of the electron-transfer resistance derived from the impedance spectra upon variation of the pH value: (i) the first run of the pH value in the acidic direction (●); (ii) the second run of the pH value in the basic direction (○); and (iii) the third run of the pH value in the acidic direction (□). (C) The reversible switching of the electron-transfer resistance, R_{et}, between high and low values, corresponding to the closed and open states of the interfacial chemical gate upon multiple changes of the pH value: pH 6.0 (a) and pH 1.8 (b).

in air or in a nonpolar solvent (Figure 1c). In order to be removed from the interface, the nonpolar component has to be pushed out by swelling of the polar component following exposure to an acidic pH. After the second titration experiments, the polar and nonpolar components of the brush are equilibrated with the aqueous environment having the specific pH value. This result is in a good agreement with the phenomena observed by AFM and contact angle measurements. The reorganization of the nanostructured polymer brushes upon changes in the pH value results in the reversible shrinking and swelling of the brush. This corresponds to the closing and opening of the chemical gate on the interface (Figures 10C and 1e,f). It should be noted that the range of electron-transfer resistance changes is significantly larger for the bicomponent mixed polymer brush compared to the monocomponent brush. Most of this difference corresponds to the closed state of the gate (the maximum value of R_{et} is *ca.* 1350 Ω for the mixed brush and *ca.* 610 Ω for the monocomponent brush). This can be easily rationalized by taking into account the fact that the nonpolar component of the mixed brush contributes to the high electron-transfer resistance in the closed state of the chemical gate, resulting in 2-fold higher resistance for the interfacial electron transfer compared to that in the monocomponent brush.

In order to elucidate the mechanism responsible for the dependence of the electron-transfer resistance on the pH value, we studied the monocomponent PDMS brush-modified ITO electrode. The Faradaic impedance spectra obtained at neutral and acidic pH values (pH 6.4 and pH 1.8) did not show any significant difference (see Supporting Information). This result corresponds to the lack of functional groups capable of dissociating (or being protonated) in the polymer molecule. Thus, this polymer cannot respond by shrinking or swelling in response to changes in pH, unlike the P2VP-containing brushes.

Investigation of the effects of grafting density and brush composition on gating was beyond the scope of the present work. However, we can discuss some aspects of these topics. The gating effect depends on the size of ions diffusing to the electrode surface. Thus, grafting density could dramatically affect transport of macroions (polyelectrolytes, DNA, proteins). In this case, gating may be broken down even at a relatively low grafting density. However, we may speculate that transport of the most common "small" ions (*e.g.*, metal ions, organic molecules, oligonucleotides) will be less affected by grafting density. This speculation originates from the fact that, even at high grafting densities approached by "grafting from" methods used for brush synthesis ($\Sigma > 10$),[65] the grafted chains grow on the solid surface by addition of monomer units to the reactive sites located on the solid surface. Consequently, the monomer molecules diffuse through the swollen brush to the reactive sites. This fact provides a strong argument for the statement that a swollen polymer brush is permeable for "small" molecules. The phase transitions for polymer brushes and mixed polymer brushes were reported for a broad range of grafting densities, including very high grafting densities.[22,39,49,52] Consequently, gating based on the transition between swollen and collapsed structures of a polymer brush can be explored in very broad range of grafting densities.

Composition of the mixed brush plays an important role in gating. The observed difference between the homopolymer brush and the mixed brush shows that the broader variation of ion transport in the mixed brush is due to the specific morphology of the mixed brush. The collapsed PDMS domains serve as a screen for a large fraction of the electrode surface, while P2VP domains serve as nanovalves. These nanovalves regulate transport of ions by swelling/shrinking the P2VP chains. Changes in the mixed brush composition will shift the balance between these two types of nanodomains.

The nanovalves in the mixed brush regulate transport of ions more efficiently than the homopolymer brush film. We may speculate that, in a homopolymer brush, different kinds of fluctuations in the grafting density naturally occurring in the course of the brush sample preparation result in the formation of "leaking points". This heterogeneous morphology is amplified when the brush shrinks in the conditions of poor solvent due to the formation of domains with high and low concentrations of P2VP chains. Hence, ions leak into the collapsed homopolymer brush through the domains with a low grafting density. In other words, gating mechanisms with nanostructured mixed polymer brushes are less sensitive to the grafting density fluctuations. We may speculate that this advantage of the mixed brush may diminish with increasing P2VP fraction due to the higher probability for the formation of the leaking points in bigger P2VP domains.

CONCLUSIONS

The switchable mixed polymer brush demonstrates excellent gating properties due to the regulation of ion transport through nanoscopic domains that are reversibly formed in the nanostructured thin film in response to external stimuli. The systems described in this report represent switchable/tunable matrices that are controlled by changes in pH. These systems can likely be exploited as chemical gates (switches) in microfluidic devices and at interfaces controlling the access of chemicals to reactive interfaces (*e.g.*, at biocatalytic surfaces in electrochemical biosensors and biofuel cells). The study of such "smart" responsive materials is underway in our laboratories.

METHODS

Materials. Aminopropyl-terminated PDMS (PDMS-NH_2, M_w = 30 000 g/mol; radius of gyration in the melt, $\langle s^2\rangle^{1/2}$ = 3.8 nm[66]) was purchased from Gelest Inc., and carboxy-terminated P2VP (P2VP-COOH, M_w = 56 000 g/mol; radius of gyration in θ-solvent, $\langle s^2\rangle^{1/2}$ = 6 nm, estimated from the dynamic light scattering in benzene at 11 °C) was purchased from Polymer Source Inc. Toluene (Sigma-Aldrich) was distilled after drying over sodium. 2-Butanone (methyl ethyl ketone, MEK), dichloromethane, NH_4OH, and H_2O_2 were used as received from Sigma-Aldrich. Highly polished silicon wafers (purchased from Semiconductor Processing, Union Miniere USA Inc.) were first cleaned in an ultrasonic bath for 30 min with dichloromethane, then placed in a cleaning solution (prepared from NH_4OH and H_2O_2) at 60 °C for 1 h, and finally rinsed several times with Millipore water (18 $M\Omega \cdot gcm^{-1}$). ITO glass was purchased from Sigma-Aldrich and cleaned using the same procedure as for the Si wafers. 3-Glycidoxypropyl trimethoxysilane (GPS) was purchased from Gelest Inc. and used as received.

Preparation of the Mixed Brushes. Polymer brushes were grafted to the surface of the ITO glass substrates and Si wafers. Samples prepared on the ITO glass were used for electrochemical experiments. Samples prepared on the surface of the Si wafers were used for AFM experiments since the roughness of ITO glass is relatively high for these investigations. Both series of samples were synthesized intact in the same reactor and were characterized with ellipsometry, contact angle experiments, and AFM scratch test (see below). We did not observe any difference in the properties of the brushes prepared on the different substrates.

For the synthesis of the mixed polymer brushes, we explored the "grafting to" method of grafting of an end-terminated polymer from the melt.[67] GPS was chemisorbed on the surface of the cleaned Si wafers or ITO glass substrate from 1% solution in dried toluene for 16 h at room temperature. Afterward, the reaction samples were carefully rinsed with toluene and ethanol to remove ungrafted GPS.

In the next step, the GPS-modified Si wafer was immersed in a bath containing liquid PDMS-NH_2. The bath was thermostatted at 70 °C for 40 min. The reference homopolymer brush was prepared by grafting at 70 °C overnight. Afterward, the nongrafted polymer was removed by rinsing the samples in toluene multiple times.

The second polymer, P2VP-COOH, was then deposited by spin-coating on the PDMS-modified Si wafer/ITO glass from a 1% solution in MEK. The grafting was performed at 130 °C overnight. The ungrafted polymers were removed by multiple rinses with water, acidic water at pH 3, and MEK. The homopolymer P2VP brush was grafted by casting a 1% polymer solution in MEK onto the surface of the GPS-modified Si wafer/ITO glass, followed by heating at 130 °C overnight. The ungrafted polymer was removed by multiple rinses with water, acidic water at pH 3, and MEK. Each step was monitored with ellipsometry, AFM, and contact angle measurements.

Sample Characterization. ***Ellipsometry.*** The layer thickness and the amount of grafted material were evaluated at 633 nm and an angle of incidence of 70° for the Si wafers and 60° for the ITO glass using an Optrel Multiscop (Berlin, Germany) null ellipsometer equipped with an *XY*-positioning table for mapping of the sample surface (lateral resolution is defined by the beam spot of about 2 mm). The measurements were performed for each sample after each step of the modification in order to use the measurements of the previous step as a reference for the simulation of ellipsometric data. In the case of the Si wafers, the initial thickness of the native SiO_2 layer (usually 1.4 ± 0.2 nm) was calculated at refractive indexes $n = 3.858 - i0.018$ for the Si substrate and n = 1.4598 for the SiO_2 layer; the ITO coating was measured to be 80 nm thick, and the refractive indexes used were 1.52 and 1.856 for the glass and ITO coatings, respectively. The thickness of the GPS layer (typically 1.0 ± 0.1 nm) was evaluated using the two-layer model: SiO_2/GPS (or ITO/GPS) for a GPS refractive index equal to 1.429. The thickness of PDMS-NH_2 as the first grafted layer (typically 1–4 nm) was evaluated with the three-layer model of SiO_2 (or ITO)/GPS/PDMS-NH_2, with n = 1.405 for the organic layer or, in the case of SiO_2(ITO)/GPS/P2VP, n = 1. 59. Finally, the thickness of the whole polymer film (typically 4–7 nm) after grafting of the second polymer was calculated using the two-layer model of SiO_2(ITO)/polymer, considering the thin polymer film as an effective optical medium with n = 1.5. We estimated that this calculation results in an error no larger than ±5% for the 5 nm thick films since the difference in the refractive indexes of all the organic ingredients is small. From the obtained values, we calculated the grafting amount of each polymer, $A = H\rho$, and the grafting density, $\sigma = AN_A/M_w$, where H is the ellipsometric thickness of the dry sample of the brush, ρ is the density of the polymer (ρ = 0.98 $g \cdot cm^{-3}$ for PDMS and 1.17 $g \cdot cm^{-3}$ for P2VP), N_A is Avogadro's number, and M_w is the molecular weight. The thickness of films swollen in water was measured in a sample liquid cell with a tube design (the extension tubes are fixed tubes on the laser and detector-arm of the Multiskop and were dipped into the sample liquid cell).[68] The swollen layer thickness was calculated using the two-layer model of SiO_2(ITO)/swollen polymer, considering the swollen polymer film as an effective optical medium with n = 1.4. We estimated that this calculation results in an error no larger than ±10% for the three-times swollen films in water.

Atomic Force Microscopy. AFM studies were performed on a Dimension 3100 microscope for dry samples and MultiMode microscopes (Veeco, Plainview, NY) in the liquid cell. The tapping mode was used to map the film morphology at ambient conditions and in water. AFM tips of Veeco NP and Veeco DNP with a resonance frequency of 75 kHz and a spring constant of 0.58–0.32 N/m were used at ambient conditions. AFM tips of BS-Tap 300 with a resonance frequency of 300 kHz and a spring constant of 40 N/m were used in water. The root-mean-square (rms) roughness for all samples was calculated over the 2 × 2 μm^2 scanned area using commercial software. The force–distance curves in water were recorded with functionalized AFM tips with primary amino groups (Novascan Technologies, Inc., Ames, IA) of 42 nm curvature radius and 0.12 N/m spring constant. For each set of conditions, we recorded about 250 force–distance curves.

Software for the subtraction of AFM images was written in the Borland C++ Builder 6.0 environment. The subtracted AFM image was obtained as the difference between two AFM data matrices after the alignment of the images and accounting for thermal or mechanical drift along the slow and fast scan axes. AFM data matrices were loaded from a WSxM software format and exposed on screen as raster images for the operator's convenience. Positioning, scaling, and skewing of the minuend AFM data image allowed it to be aligned with respect to the subtrahend AFM data image with the resolution of single data points. Algorithms commonly applied for the processing of raster images were used: up-scaling was calculated by a bilinear averaging algorithm; skewing was performed by linear averaging; down-scaling was done by fractional averaging.

Contact Angle. The wettability of the surfaces was characterized by contact angle measurements of sessile water droplets using a homemade system, which included a sample stage, a long focus microscope, a source of light, a charge-coupled device camera, a personal computer, and self-coded software for processing drop images. Advancing (adv) and receding (rec) contact angles from six individual drops placed on six new surface areas were measured by adding or withdrawing a small volume of water through a syringe. The needle was maintained in contact with the drop during the experiments. All readings were then averaged to give a mean advancing and receding contact angle for each sample. The accuracy of this technique is in the order of ±2°.

Electrochemical Measurements. Faradaic impedance spectroscopy measurements were performed using an electrochemical analyzer (Autolab PGSTAT12, EcoChemie B.V., Utrecht, Netherlands). The measurements were carried out at ambient temperature (23 ± 2 °C) in a conventional electrochemical cell consisting of the polymer brush-modified ITO electrode as a working electrode (1 cm × 1 cm area exposed to the solution), a Pt-grid auxiliary electrode, and a saturated Ag/AgCl reference electrode. All potentials are reported relative to this reference electrode. The cell was placed in a grounded Faraday cage. The Faradaic impedance measurements were performed in 0.1 M Na_2SO_4 solu-

tion with the pH value adjusted by addition of diluted H_2SO_4 or NaOH directly in the electrochemical cell in the presence of a $K_3[Fe(CN)]_6$:$K_4[Fe(CN)_6]$ 1:1 mixture (10 mM) as a redox probe. The Faradaic impedance spectra were recorded while applying a bias potential that equaled the redox-probe formal potential, 0.17 V, and using a 5 mV alternative voltage in the frequency range 10 mHz–10 kHz. The Faradaic impedance spectra were plotted in the form of complex plane diagrams (Nyquist plots). The experimental impedance spectra were fitted using electronic equivalent circuits in order to derive the electron-transfer resistance (R_{et}) values. For this purpose, commercial software (ZView, version 2.1b, Scribner Associates, Inc., Southern Pines, NC) was employed.

Acknowledgment. We thank Dr. Yuri Roiter for the subtraction software and assistance in the subtraction of the AFM images. We acknowledge NSF awards DMR 0706209 and DMR 0602528 for the financial support of this work.

Supporting Information Available: Faradaic impedance spectra of the PDMS brush-modified ITO electrode obtained at neutral and acidic pH values. This material is available free of charge *via* the Internet at http://pubs.acs.org.

REFERENCES AND NOTES

1. O'Rourke, B. Mitochondrial Ion Channels. *Annu. Rev. Physiol.* **2007**, *69*, 19–49.
2. Defelice, L. J.; Goswami, T. Transporters as Channels. *Annu. Rev. Physiol.* **2007**, *69*, 87–112.
3. Catterall, W. A.; Hulme, J. T.; Jiang, X.; Few, W. P. Review—Regulation of Sodium and Calcium Channels by Signaling Complexes. *J. Recept. Signal Transduction* **2006**, *26*, 577–598.
4. Roux, B. Ion Conduction and Selectivity in K^+ Channels. *Annu. Rev. Biophys. Biomol. Struct.* **2005**, *34*, 153–171.
5. Scholz-Starke, J.; Gambale, F.; Carpaneto, A. Modulation of Plant Ion Channels by Oxidizing and Reducing Agents. *Arch. Biochem. Biophys.* **2005**, *434*, 43–50.
6. Doyle, D. A. Molecular Insights into Ion Channel Function. *Mol. Membr. Biol.* **2004**, *21*, 221–225.
7. Kinoshita, T. Biomembrane Mimetic Systems. *Prog. Polym. Sci.* **1995**, *20*, 527–583.
8. Janshoff, A.; Steinem, C. Scanning Force Microscopy of Artificial Membranes. *ChemBioChem* **2001**, *2*, 799–808.
9. Besanger, T. R.; Brennan, J. D. Entrapment of Membrane Proteins in Sol-Gel Derived Silica. *J. Sol-Gel Sci. Technol.* **2006**, *40*, 209–225.
10. Schuster, B.; Sleytr, U. B. Biomimetic S-Layer Supported Lipid Membranes. *Curr. Nanosci.* **2006**, *2*, 143–152.
11. Sharma, M. K.; Gilchrist, M. L. Templated Assembly of Biomembranes on Silica Microspheres Using Bacteriorhodopsin Conjugates as Structural Anchors. *Langmuir* **2007**, *23*, 7101–7112.
12. Peteu, S. F. Responsive Materials Configured for Micro- and Nanoactuation. *J. Intell. Mater. Syst. Struct.* **2007**, *18*, 147–152.
13. Davis, A. P.; Sheppard, D. N.; Smith, B. D. Development of Synthetic Membrane Transporters for Anions. *Chem. Soc. Rev.* **2007**, *36*, 348–357.
14. Sisson, A. L.; Shah, M. R.; Bhosale, S.; Matile, S. Synthetic Ion Channels and Pores. *Chem. Soc. Rev.* **2006**, *35*, 1269–1286.
15. Banghart, M. R.; Volgraf, M.; Trauner, D. Engineering Light-Gated Ion Channels. *Biochemistry* **2006**, *45*, 15129–15141.
16. Baker, L. A.; Choi, Y. S.; Martin, C. R. Nanopore Membranes for Biomaterials Synthesis, Biosensing and Bioseparations. *Curr. Nanosci.* **2006**, *2*, 243–255.
17. Hector, R. S.; Gin, M. S. Signal-Triggered Transmembrane Ion Transport through Synthetic Channels. *Supramol. Chem.* **2005**, *17*, 129–134.
18. Milner, S. T. Polymer Brushes. *Science* **1991**, *251*, 905–914.
19. Usov, D.; Gruzdev, V.; Nitschke, M.; Stamm, M.; Hoy, O.; Luzinov, I.; Tokarev, I.; Minko, S. Three-Dimensional Analysis of Switching Mechanism of Mixed Polymer Brushes. *Macromolecules* **2007**, *40*, 8774–8783.
20. Luzinov, I.; Minko, S.; Tsukruk, V. V. Adaptive and Responsive Surfaces Through Controlled Reorganization of Interfacial Polymer Layers. *Prog. Polym. Sci.* **2004**, *29*, 635–698.
21. Minko, S. Responsive Polymer Brushes. *J. Macromol. Sci., Polym. Rev.* **2006**, *46*, 397–420.
22. Minko, S.; Muller, M.; Usov, D.; Scholl, A.; Froeck, C.; Stamm, M. Lateral versus Perpendicular Segregation in Mixed Polymer Brushes. *Phys. Rev. Lett.* **2002**, *88*. Art. No. 035502.
23. Minko, S.; Usov, D.; Goreshnik, E.; Stamm, M. Environment-Adopting Surfaces with Reversibly Switchable Morphology. *Macromol. Rapid Commun.* **2001**, *22*, 206–211.
24. Santer, S.; Kopyshev, A.; Yang, H. K.; Ruhe, J. Local Composition of Nanophase-Separated Mixed Polymer Brushes. *Macromolecules* **2006**, *39*, 3056–3064.
25. Zhao, B.; Haasch, R. T.; Maclaren, S. Solvent-Induced Self-Assembly of Mixed Poly(Methyl Methacrylate)/Polystyrene Brushes on Planar Silica Substrates: Molecular Weight Effect. *J. Am. Chem. Soc.* **2004**, *126*, 6124–6134.
26. Julthongpiput, D.; Lin, Y. H.; Teng, J.; Zubarev, E. R.; Tsukruk, V. V. Y-Shaped Polymer Brushes: Nanoscale Switchable Surfaces. *Langmuir* **2003**, *19*, 7832–7836.
27. Motornov, M.; Sheparovych, R.; Tokarev, I.; Roiter, Y.; Minko, S. Nonwettable Thin Films from Hybrid Polymer Brushes Can Be Hydrophilic. *Langmuir* **2007**, *23*, 13–19.
28. Houbenov, N.; Minko, S.; Stamm, M. Mixed Polyelectrolyte Brush from Oppositely Charged Polymers for Switching of Surface Charge and Composition in Aqueous Environment. *Macromolecules* **2003**, *36*, 5897–5901.
29. Usov, D.; Nitschke, M.; Chitry, V.; Ulbrich, K.; Minko, S.; Stamm, M. Mixed Polymer Brushes with Thermal Response Amplified by Roughness. Presented at the 227th ACS National Meeting, Anaheim, CA, March 28–April 1, 2004; Abstract PMSE-364.
30. Motornov, M.; Sheparovych, R.; Lupitskyy, R.; Macwilliams, E.; Hoy, O.; Luzinov, I.; Minko, S. Stimuli-Responsive Colloidal Systems From Mixed-Brush Coated Nanoparticles. *Adv. Funct. Mater.* **2007**, *17*, 2307–2314.
31. Ionov, L.; Houbenov, N.; Sidorenko, A.; Stamm, M.; Minko, S. Smart Microfluidic Channels. *Adv. Funct. Mater.* **2006**, *16*, 1153–1160.
32. Ionov, L.; Minko, S.; Stamm, M.; Gohy, J. F.; Jerome, R.; Scholl, A. Reversible Chemical Patterning on Stimuli-Responsive Polymer Film: Environment-Responsive Lithography. *J. Am. Chem. Soc.* **2003**, *125*, 8302–8306.
33. Balazs, A. C.; Singh, C.; Zhulina, E.; Chern, S. S.; Lyatskaya, Y.; Pickett, G. Theory of Polymer Chains Tethered At Interfaces. *Prog. Surf. Sci.* **1997**, *55*, 181–269.
34. Motornov, M.; Sheparovych, R.; Lupitskyy, R.; Macwilliams, E.; Minko, S. Responsive Colloidal Systems: Reversible Aggregation and Fabrication of Superhydrophobic Surfaces. *J. Colloid Interface Sci.* **2007**, *310*, 481–488.
35. Minko, S.; Müller, M.; Motornov, M.; Nitschke, M.; Grundke, K.; Stamm, M. Two-Level Structured Self-Adaptive Surfaces with Reversibly Tunable Properties. *J. Am. Chem. Soc.* **2003**, *125*, 3896–3900.
36. Uhlmann, P.; Ionov, L.; Houbenov, N.; Nitschke, M.; Grundke, K.; Motornov, M.; Minko, S.; Stamm, M. Surface Functionalization by Smart Coatings: Stimuli-Responsive Binary Polymer Brushes. *Prog. Org. Coat.* **2006**, *55*, 168–174.
37. Motornov, M.; Minko, S.; Eichhorn, K. J.; Nitschke, M.; Simon, F.; Stamm, M. Reversible Tuning of Wetting Behavior of Polymer Surface with Responsive Polymer Brushes. *Langmuir* **2003**, *19*, 8077–8085.
38. Uhlmann, P.; Houbenov, N.; Brenner, N.; Grundke, K.; Burkert, S.; Stamm, M. In-Situ Investigation of the Adsorption of Globular Model Proteins on Stimuli-Responsive Binary Polyelectrolyte Brushes. *Langmuir* **2007**, *23*, 57–64.
39. Santer, S.; Ruhe, J. Motion of Nano-Objects on Polymer Brushes. *Polymer* **2004**, *45*, 8279–8297.

40. Zhou, F.; Hu, H. Y.; Yu, B.; Osborne, V. L.; Huck, W. T. S.; Liu, W. M. Probing the Responsive Behavior of Polyelectrolyte Brushes Using Electrochemical Impedance Spectroscopy. *Anal. Chem.* **2007**, *79*, 176–182.
41. Choi, E.-Y.; Azzaroni, O.; Cheng, N.; Zhou, F.; Kelby, T.; Huck, W. T. S. Electrochemical Characteristics of Polyelectrolyte Brushes with Electroactive Counterions. *Langmuir* **2007**, *23*, 10389–10394.
42. Szleifer, I.; Carignano, M. A. Tethered Polymer Layers. *Adv. Chem. Phys.* **1996**, *94*, 165–260.
43. Brown, G.; Chakrabarti, A.; Marko, J. F. Microphase Separation of a Dense 2-Component Grafted-Polymer Layer. *Europhys. Lett.* **1994**, *25*, 239–244.
44. Lai, P. Y. Binary Mixture of Grafted Polymer Chains: A Monte Carlo Simulation. *J. Chem. Phys.* **1994**, *100*, 3351–3357.
45. Soga, K. G.; Zuckermann, M. J.; Guo, H. Binary Polymer Brush in a Solvent. *Macromolecules* **1996**, *29*, 1998–2005.
46. Marko, J. F.; Witten, T. A. Phase Separation in a Grafted Polymer Layer. *Phys. Rev. Lett.* **1991**, *66*, 1541–1544.
47. Zhulina, E.; Balazs, A. C. Designing Patterned Surfaces by Grafting Y-Shaped Copolymers. *Macromolecules* **1996**, *29*, 2667–2673.
48. Muller, M. Phase Diagram of a Mixed Polymer Brush. *Phys. Rev. E* **2002**, *65*, 30802.
49. Sidorenko, A.; Minko, S.; Schenk-Meuser, K.; Duschner, H.; Stamm, M. Switching of Polymer Brushes. *Langmuir* **1999**, *15*, 8349–8355.
50. Minko, S.; Patil, S.; Datsyuk, V.; Simon, F.; Eichhorn, K. J.; Motornov, M.; Usov, D.; Tokarev, I.; Stamm, M. Synthesis of Adaptive Polymer Brushes via Grafting to Approach from Melt. *Langmuir* **2002**, *18*, 289–296.
51. Lemieux, M.; Minko, S.; Usov, D.; Stamm, M.; Tsukruk, V. V. Direct Measurement of Thermoelastic Properties of Glassy and Rubbery Polymer Brush Nanolayers Grown by Grafting-from Approach. *Langmuir* **2003**, *19*, 6126–6134.
52. Santer, S.; Kopyshev, A.; Donges, J.; Ruhe, J.; Jiang, X. G.; Zhao, B.; Muller, M. Memory of Surface Patterns in Mixed Polymer Brushes: Simulation and Experiment. *Langmuir* **2007**, *23*, 279–285.
53. Ruhe, J.; Ballauff, M.; Biesalski, M.; Dziezok, P.; Gröhn, F.; Johannsmann, D.; Houbenov, N.; Hugenberg, N.; Konradi, R.; Minko, S.; *et al.* In *Polyelectrolytes With Defined Molecular Architecture I*; Schmidt, M., Ed.; Springer: New York, 2004; pp 79–150.
54. Williams, D. R. M. Grafted Polymers in Bad Solvents: Octopus Surface Micelles. *J. Phys. II France* **1993**, *3*, 1313–1318.
55. Cappella, B.; Dietler, G. Force−Distance Curves by Atomic Force Microscopy. *Surf. Sci. Rep.* **1999**, *34*, 1–104.
56. Bard, A. J.; Faulkner, L. R. *Electrochemical Methods: Fundamentals and Applications*; Wiley: New York, 1980.
57. Stoynov, Z. B.; Grafov, B. S.; Savova-Stoynova, B. S.; Elkin, V. V. *Electrochemical Impedance*; Nauka: Moscow, 1991.
58. Katz, E.; Willner, I. Probing Biomolecular Interactions at Conductive and Semiconductive Surfaces by Impedance Spectroscopy: Routes to Impedimetric Immunosensors, DNA-Sensors, and Enzyme Biosensors. *Electroanalysis* **2003**, *15*, 913–947.
59. Peng, D. K.; Yu, S. T.; Alberts, D. J.; Lahann, J. Switching the Electrochemical Impedance of Low-Density Self-Assembled Monolayers. *Langmuir* **2007**, *23*, 297–304.
60. Tagliazucchi, M. E.; Calvo, E. J. Surface Charge Effects on the Redox Switching of Self-Assembled Redox Polyelectrolyte Multilayers. *J. Electroanal. Chem.* **2007**, *599*, 249–259.
61. Zhou, J. H.; Wang, G.; Hu, J. Q.; Lu, X. B.; Li, J. H. Temperature, Ionic Strength and pH Induced Electrochemical Switching of Smart Polymer Interfaces. *Chem. Commun.* **2006**, 4820–4822.
62. Randles, J. E. B. Kinetics of Rapid Electrode Reactions. *Discuss. Faraday Soc.* **1947**, *1*, 11–19.
63. Ershler, B. V. Impedance Analysis of Electrochemical Reactions. *Discuss. Faraday Soc.* **1947**, *1*, 269–277.
64. Bardea, A.; Katz, E.; Willner, I. Probing Antigen−Antibody Interactions on Electrode Supports by the Biocatalyzed Precipitation of an Insoluble Product. *Electroanalysis* **2000**, *12*, 1097–1106.
65. Brittain, W. J.; Minko, S. A Structural Definition of Polymer Brushes. *J. Polym. Sci., Part A* **2007**, *45*, 3505–3512.
66. Arrighi, V.; Gagliardi, S.; Dagger, A.; Shenton, M. *ISIS Facility Annual Report*; Rutherford Appleton Laboratory: Edinburgh, UK, 2000;Report No. 10229 (www.isis.rl.ac.uk/isis2000/reports/10929).
67. Luzinov, I.; Julthongpiput, D.; Malz, H.; Pionteck, J.; Tsukruk, V. V. Polystyrene Layers Grafted to Epoxy-Modified Silicon Surfaces. *Macromolecules* **2000**, *33*, 1043–1048.
68. Benjamins, J. W.; Jonsson, B.; Thuresson, K.; Nylander, T. New Experimental Setup To Use Ellipsometry To Study Liquid−Liquid and Liquid−Solid Interfaces. *Langmuir* **2002**, *18*, 6437–6444.